HOKKAIDO UNIVERSITY

Title	Anisotropic Heat Conduction in Ion - Substituted Layered Cobalt Oxides
Author(s)	Cho, Hai Jun; Takashima, Yugo; Nezu, Yukio et al.
Citation	Advanced Materials Interfaces, 7(3), 1901816 https://doi.org/10.1002/admi.201901816
Issue Date	2020-02-07
Doc URL	https://hdl.handle.net/2115/80379
Rights	This is the peer reviewed version of the following article: Cho, H. J., Takashima, Y., Nezu, Y., Onozato, T., Ohta, H., Anisotropic Heat Conduction in Ion - Substituted Layered Cobalt Oxides. Adv. Mater. Interfaces 2020, 7, 1901816, which has been published in final form at https://doi.org/10.1002/admi.201901816 . This article may be used for non-commercial purposes in accordance with Wiley Terms and Conditions for Use of Self-Archived Versions.
Type	journal article
File Information	(Final) Manuscript_Anisotropic heat conduction of AxCoO2.pdf

Hokkaido University Collection of Scholarly and Academic Papers : HUSCAP

DOI: 10.1002/((please add manuscript number))
Article type: Communication

Anisotropic Heat Conduction in Ion Substituted Layered Cobalt Oxides

Hai Jun Cho, Yugo Takashima, Yukio Nezu, Takaki Onozato, and Hiromichi Ohta**

Prof. H.J. Cho, Prof. H. Ohta
Research Institute for Electronic Science, Hokkaido University, N20W10, Kita, Sapporo 001−0020, Japan
E-mail: joon@es.hokudai.ac.jp, hiromichi.ohta@es.hokudai.ac.jp
Prof. H.J. Cho, Y. Takashima, Y. Nezu, T. Onozato, Prof. H. Ohta
Graduate School of Information Science and Technology, Hokkaido University, N14W9, Kita, Sapporo 060−0814, Japan

Keywords: anisotropy, thermal conductivity, thermoelectric properties, layered cobalt oxides, epitaxial films

Layered cobalt oxides, A_xCoO_2 (A = Li, Na, Ca, and Sr), have been attracting attention as thermoelectric materials showing large thermoelectric figure of merit $ZT = S^2 \cdot \sigma \cdot T \cdot \kappa^{-1}$ (S: thermopower, σ: electrical conductivity, T: absolute temperature, κ: thermal conductivity) at higher temperatures. Due to the layered structure, A_xCoO_2 shows strong anisotoropy in the thermoelectric properties; both S and σ are large along the layer though systemaltic study in κ has not been reported thus far. Here we systematically show the anisotropy in κ of A_xCoO_2 with the effect of A_x on κ. We fabricated A_xCoO_2 epitaxial films with two different crystallographic orientations with respect to the surface normal to the substrates and measured the κ in normal to the substrate. The κ parallel to the layers ($\kappa_{\parallel}$) was 3−6 times larger than that perpendicular to the layers ($\kappa_{\perp}$). The $\kappa_{\parallel}$ decreased with increasing the atomic mass of A_x though $\kappa_{\perp}$ was insensitive to it; anisotropy of κ was controlled by substituting heavier A_x ions. The present result would provide new materials design concept for good thermoelectric materials.

Thermoelectric energy conversion is an attractive energy harvesting technology that utilizes thermoelectric Seebeck effect of thermoelectric materials with high thermoelectric figure of

merit, ZT ($=S^2 \cdot \sigma \cdot T \cdot \kappa^{-1}$, where Z is the figure of merit, T is the absolute temperature, S is the Seebeck coefficient or thermopower, σ is the electrical conductivity, and κ is the thermal conductivity, respectively).[1-2] Today, commercially available thermoelectric devices mostly utilize heavy-metal based materials such as Bi_2Te_3 or PbTe, which exhibit high conversion efficiencies ($ZT > 1$) at moderate temperatures (100 – 400 °C).[2-3] However, they have several issues including high cost, toxicity,[4] and poor chemical/thermal stabilities.[5] Therefore, researchers have been searching for alternate high-ZT thermoelectric materials that are cost-effective and stable at elevated temperatures.

Na_xCoO_2 is known as one of the promising candidate of thermoelectric materials because single crystalline Na_xCoO_2 (bulk and film) shows a large thermoelectric power factor (PF = $S^2 \cdot \sigma$) [6-10], which are attributed to strongly correlated d-electrons in the CoO_2 layers.[11-18] In addition, its ZT is maximized at elevated temperatures (> 500 ^oC) [7]. However, Na_xCoO_2 has several practical issues for thermoelectric applications, including low thermal stability, high sensitivity to moisture due to the Na^+ ions.[18-21] Since the crystal structure of A_xCoO_2 is a layered structure, composed of the edge sharing CoO_6 octahedron layers separated by monolayers of A_x ions alternately stacked along with the c-axis, there were many attempts to replace the Na^+ ions with heavier ions to improve the chemical stability.[22-24] While this approach indeed improved the chemical stability, substituting Na^+ ions often reduced the PF,[25-27] and very few substitutions were accompanied by improvements in the PF.

In this study, we focus on the potential of layered cobalt oxides A_xCoO_2 as thermoelectric materials because Na_xCoO_2, one of its members, is a promising thermoelectric material. While the electrons in A_x layers are not significantly involved in thermoelectric properties, the A_x layers themselves can interact with the CoO_2 layers and affect the electron transport properties of the entire lattice. Thus, the thermoelectric properties of A_xCoO_2 are highly

versatile as they can be engineered by modifying the A_x layers (type of ions, planar densities),[8, 20, 24, 28-35] and understanding this versatility is of great value for developing efficient thermoelectric materials as well as enhancing the fundamental knowledge in layered structures.

Investigating the κ of A_xCoO_2 is just as important as examining the PF since the thermal conductivity (κ) also plays a critical role in the figure of merit ($ZT = S^2 \cdot \sigma \cdot T \cdot \kappa^{-1}$). Like conventional oxides, the conduction of heat in A_xCoO_2 is dominated by phonons, and the effect of A_x was analyzed with *ab-initio* calculations.[36-37] In heat transport properties, the effect of A_x is dominated by the mass A ions and their planar densities, which affect the impedance mismatch between A_x and CoO_2 layers and control the overlap between the vibrational density of states. These calculations suggest that the in-plane κ of A_xCoO_2 can potentially be reduced without sacrificing the power factor. Unfortunately, due to the strong anisotropy in layered structures and difficulties in preparing appropriate specimens for κ measurements, experimentally measured κ of A_xCoO_2 is limited to polycrystalline or uniaxial values.[8, 24, 28, 35, 38] The anisotropic κ of A_xCoO_2 has not been experimentally and clearly investigated in detail to date, and this is the context of this research.

In order to overcome the difficulties in preparing large bulk single crystals for κ measurements, differently oriented epitaxial films were used,[9, 31, 39] and the anisotropy was numerically analyzed from the κ values measured by time-domain thermoreflectance (TDTR). Here we experimentally show the crystallographic anisotropy of κ in A_xCoO_2 (A = Li, Na, Ca, and Sr) and the effect of A_x on κ. For all films, κ parallel to the layers ($\kappa_{||}$) was greater than κ perpendicular to the layers ($\kappa_{\perp}$), and the $\kappa_{||}$ values were significantly reduced with increasing the A_x mass. These results experimentally confirm that controlling the A_x planes is an effective

approach for optimizing the *ZT* of A_xCoO_2. The simple analysis on the anisotropic κ in this study can be applied to other layered structures or material systems.

The A_xCoO_2 (*A* = Li, Na, Ca, and Sr) films were heteroepitaxially grown on sapphire substrates using the reactive solid-phase epitaxy (R-SPE) method[9, 39] followed by the ion-exchange method.[20, 26, 31] The detailed sample preparation can be found in the **Experimental Section**. On (0001) α-Al_2O_3 substrates (C-sapphire, hereafter), the A_x/CoO_2 layers of the films were parallel to the substrate surface, but the inclination of the layers changed to 43 ° on $(1\bar{1}00)$ α-Al_2O_3 substrates (M-sapphire, hereafter) (**Fig. 1**). The X-ray diffraction (XRD) patterns of the resultant films (**Supplementary Fig. S1**) clearly show that $LiCoO_2$ [40], $Ca_{0.33}CoO_2$ [27], $Sr_{0.33}CoO_2$ [25], and $Na_{0.8}CoO_2$ [9] were heteroepitaxially grown on the sapphire substrates since the peak locations are consistent with previous studies. Strong film peak intensities suggest that the films have high crystallinity, and no additional peaks from impurities were detected. Surface morphologies obtained from atomic force microscopy (AFM) show plate-like grains with stepped and terraced structures for films on C-sapphire substrates while the surfaces of inclined films reveal straight stripes along with the *x*-direction, which are expected from the cross-section of layered structures (**Fig. 2**). All structural characterizations indicate excellent film qualities and strong orientations.

The TDTR signals from the films and the observed κ (κ_{obsd}) values from the simulation are shown in **Fig. 3**. The film thickness (*t*) measured from X-ray reflectivity (data not shown) is also shown. As expected from the anisotropic structure, the decay characteristics of the films strongly depend on the orientations. Regardless of the A_x layers, the inclined films on M-sapphire substrates exhibited faster signal decay. This suggests $\kappa_{||} > \kappa_{\perp}$ in A_xCoO_2, which perhaps should not be surprising. κ_{obsd} can be numerically expressed by **Eq. 1** below:

$$\kappa_{obsd} = \sqrt{\kappa_{\parallel}{}^2 cos^2\theta + \kappa_{\perp}{}^2 sin^2\theta} \qquad (1)$$

where θ is the incline angle of the layers with respect to the substrate surface. For example, θ = 90 ° and $\kappa_{obsd} = \kappa_{\perp}$ for C-sapphire oriented films. In case of M-sapphire oriented films, θ = 90 ° − 43 ° = 47 °. The anisotropy in the planar directions was confirmed to be not significant by *ab-initio* calculations.[36-37] The derivation for **Eq. 1** is available in the **Supplementary Fig. S2**. More generalized expression in tensor form can be found elsewhere.[41]

The $\kappa_{\perp}$ and $\kappa_{||}$ of A_xCoO_2 calculated from **Eq. 1** are summarized in **Table I**, which show that the κ of A_xCoO_2 can be controlled by ion substitutions without drastically changing the thermoelectric power factor (PF) (**Supplementary Fig. S4**). The $\kappa_{||}$ was higher than $\kappa_{\perp}$ in all films, which is consistent with previous results from ab-initio calculations [42-43]. The measured thermal conductivity values in this study are low compared to the computational results. It is difficult to direct comment on this discrepancy at this stage, but it can be attributed to structural defects in the films [44-45] or limitations in applying computational results (bulk single crystal) to thin films. $LiCoO_2$ exhibited the highest κ in all directions while $Ca_{0.33}CoO_2$ shows the strongest anisotropy ($\kappa_{||}/\kappa_{\perp} \approx 6.2$). In the planar direction ($\kappa_{||}$), from the highest to lowest, the layered cobalt oxides measured in this study are listed as $LiCoO_2 \rightarrow Ca_{0.33}CoO_2 \rightarrow Na_{0.8}CoO_2 \rightarrow Sr_{0.33}CoO_2$. In the perpendicular direction ($\kappa_{\perp}$), from the highest to lowest, the list goes as $LiCoO_2 \rightarrow Na_{0.8}CoO_2 \rightarrow Sr_{0.33}CoO_2 \rightarrow Ca_{0.33}CoO_2$. In general, the differences observed in $\kappa_{||}$ is much greater than those observed in $\kappa_{\perp}$. The anisotropic κ measured in this study are plotted against the average atomic mass of A_x (product of atomic mass and x) in **Fig. 4**. For comparison, results from other studies were also plotted.

Previously reported thermal conductivities of polycrystalline Na_xCoO_2 ($0.57 < x < 0.9$) [29, 32-33] lie between the $\kappa_{\perp}$ and $\kappa_{||}$ of $Na_{0.8}CoO_2$ measured in our study, which is reasonable since the

grains in polycrystalline materials are randomly oriented. $\kappa_{||}$ of the A_xCoO_2 monotonically decreases with the average atomic mass of A_x. This phenomenon reflects the effect of A_x on the impedance mismatch, which were predicted in *ab-initio* calculations.[37, 46] Heavy ions reduce lattice vibrational amplitudes and the group velocity of phonons.[47] Therefore, heavy ions in A_x layers greatly increase the impedance mismatch between the layers and decrease $\kappa_{||}$ as it becomes difficult for the vibrational modes of the layers to couple. This phenomenon seems to dominate $\kappa_{||}$ in **Fig. 4a**. If the ions in A_x layers are orders of magnitude heavier than the ions in the CoO_2 layers, the vibrational modes in the layers can be de-coupled in theory since overlap in the vibrational density of states of the layer is eliminated. While this phenomenon enhances $\kappa_{||}$,[36] it is not applicable in our case since the masses of *A* ions are on the same order. On the other hand, $\kappa_{\perp}$ did not have any noticeable correlations with the average atomic mass but monotonically decreased with *x* (**Table I**). The difference between $Ca_{0.33}CoO_2$ and $Sr_{0.33}CoO_2$ suggests that the effect of the atomic mass of *A* is small. Unlike $\kappa_{||}$, $\kappa_{\perp}$ is related to the transmission of phonons through the A_x / CoO_2 layers, and therefore, directly affected by interfacial scattering cross sections. These suggest that $\kappa_{\perp}$ of A_xCoO_2 is dominated by the vacancy scattering of phonons, which is related to the planar density of A_x.

The main objective of this work is the effect of substituting different ions in A_xCoO_2 films. While the results demonstrate that inserting heavy atoms between CoO_2 layers decreases the in-plane thermal conductivity of A_xCoO_2, we would like to note the effect of *x* remains unclear. Ions in A_x occupy the interstitial sites of the CoO_2 layers on basal planes, which exhibit a 6-fold symmetry. Ion vacancies will break the symmetry, shift the equilibrium positions, and induce vibrational anharmonicity.[37] Studies found that this phenomenon 'rattles' the vibrational modes and reduces the thermal conductivity.[33] Although this is beyond the scope of this work, it is necessary to fully understand the thermal conductivity of A_xCoO_2.

Therefore, in future, extensive structural characterization using electron microscopy will be necessary to investigate how *x* affects the structure, lattice strain, and thermal conductivity.

In summary, we developed a simple method for analyzing the thermal conductivity of layered structures and experimentally demonstrated the effect of A_x on the anisotropic thermal conductivity in layered A_xCoO_2 (A = Li, Na, Ca, and Sr). The thermal conductivity parallel to the layers was mainly controlled by the impedance mismatch between A_x and CoO_2 layers while the thermal conductivity perpendicular to the layers was affected by vacancy scatterings in A_x layers. Both factors monotonically controlled the thermal conductivities in each direction. The results of this study will be of great value in understanding fundamental heat transport properties of layered structures as well as developing A_xCoO_2 based thermoelectric materials. In addition, the analysis on the anisotropic thermal conductivity used in this study can be applied to other layered materials.

Experimental Section

Epitaxial film growth of A_xCoO_2: Epitaxial films of $Na_{0.8}CoO_2$ were prepared by the reactive solid-phase epitaxy (R-SPE) method.[9, 39] Firstly, epitaxial CoO films were grown on sapphire substrates using PLD at 600 °C. The resultant CoO films were covered with yttria-stabilized zirconia (YSZ) and then were heated with $NaHCO_3$ powders at 750 °C for 2 h, which yields $Na_{0.8}CoO_2$. The $Na_{0.8}CoO_2$ was then converted to different A_xCoO_2 using topotactic ion-exchange method. For fabricating $LiCoO_2$ films, $Na_{0.8}CoO_2$ films were heated at 260 °C for 4 h in $LiNO_3$/LiCl mixture.[26] $Ca_{0.33}CoO_2$[19] and $Sr_{0.33}CoO_2$[20] films were fabricated by heating $Na_{0.8}CoO_2$ films with $Ca(NO_3)_2$ and $Sr(NO_3)_2$ powders, respectively, at 300 °C for 5 h.

Crystallographic characterization of A_xCoO_2 epitaxial films: The crystallographic details of the films were measured with high-resolution X-ray diffraction using Cu Kα_1 (1.54059 Å)

(ATX-G, Rigaku Co.). The film thicknesses were measured from the Kiessig fringes in X-ray reflectivity (data not shown). The surface morphologies of the films were characterized with atomic force microscopy (AFM, Nanocute, Hitachi Hi-Tech Sci. Co.).

Electron transport properties measurements: The electrical resistivity (ρ) of the films was measured with the conventional dc four-probe method in van der Pauw electrode configuration. For thermopower (S) measurements, temperature differences (ΔT <2 K) were created in the films. The S values were obtained from the slope of the changes in the electromotive force with respect to the temperature difference between two ends of the films (correlation: ~99.9%). All electron transport properties were measured in vacuum to prevent the effect of moisture, and InGa alloy was used at the end of the probes to ensure Ohmic contacts.

Thermal conductivity measurements: The thermal conductivities of the A_xCoO_2 films were measured with time-domain thermoreflectance method (TDTR, PicoTR, PicoTherm Co.) The pump laser wavelength was 1550 nm, probe laser wavelength was 775 nm, pulse duration was 1 fs, pulse frequency was 20 MHz, modulation frequency was 200 kHz, respectively. Sputtered Mo (~100 nm) was used as the transducer, and the TDTR decay curves were analyzed with the simulation package provided by the manufacturer. The uncertainties were estimated from fitting errors and noises in the signal.

Supporting Information
Supporting Information is available from the Wiley Online Library or from the author.

Acknowledgements
This research was supported by Grants-in-Aid for Innovative Areas (19H05791) and Scientific Research A (17H01314) from the JSPS. H.J.C. acknowledges the support from Nippon Sheet Glass Foundation for Materials Science and Engineering. H.O. acknowledges the support from the Asahi Glass Foundation and the Mitsubishi Foundation. Student aids from the JSPS (T.O.) (17J01281) is also greatly appreciated. A part of this work was also supported by Dynamic Alliance for Open Innovation Bridging Human, Environment, and Materials, and by the Network Joint Research Center for Materials and Devices.

Conflict of Interest
The authors declare no conflict of interest.

Received: ((will be filled in by the editorial staff))
Revised: ((will be filled in by the editorial staff))
Published online: ((will be filled in by the editorial staff))

Table I. Anisotropic κ of A_xCoO_2 films observed in this study.

	$LiCoO_2$	$Na_{0.8}CoO_2$	$Ca_{0.33}CoO_2$	$Sr_{0.33}CoO_2$
$\kappa_{\perp}$ (W m^{-1} K^{-1})	3.5 $\pm$ 0.2	1.6 $\pm$ 0.1	1.1 $\pm$ 0.1	1.2 $\pm$ 0.1
$\kappa_{//}$ (W m^{-1} K^{-1})	9.2 $\pm$ 1.4	5.5 $\pm$ 0.7	6.8 $\pm$ 1.2	4.5 $\pm$ 0.7

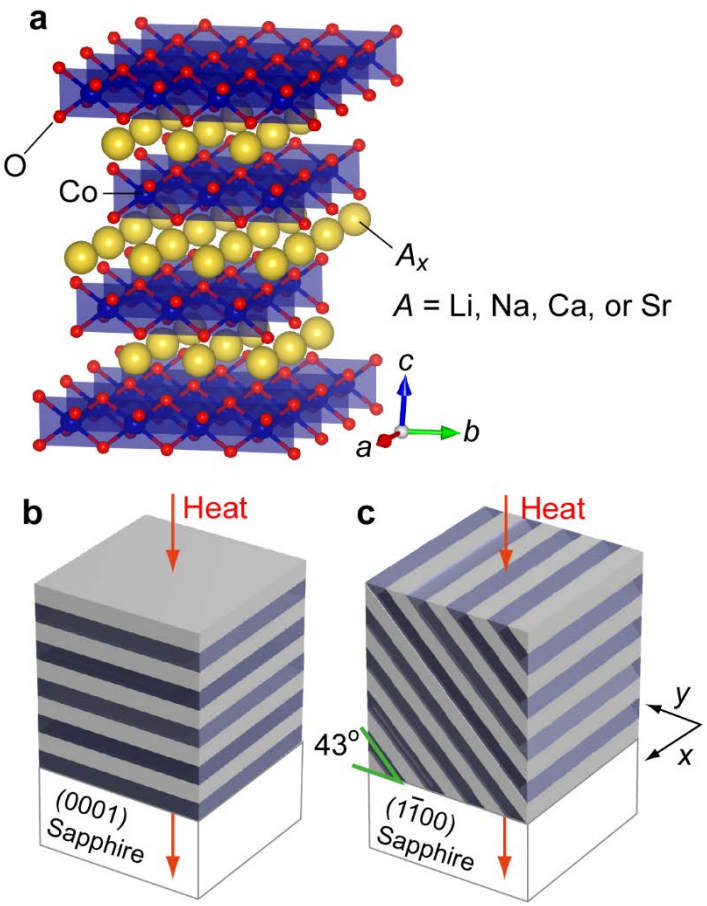

Figure 1. (a) Schematic crystal structure of A_xCoO_2 (A = Li, Na, Ca, or Sr). The planar density of A ion depends on the value of x. CoO_2 layer, composed of edge-sharing CoO_6 octahedron, and A_x layer are stacked alternately along the c-axis. (b)(c) Schematic epitaxial relationships between A_xCoO_2 and sapphire substrate grown on different crystallographic orientations of (b) C (0001) and (c) M $(1\bar{1}00)$. (b) The layers are parallel to the substrate surface. (c) The layers are inclined by 43 ° with respect to the substrate surface.

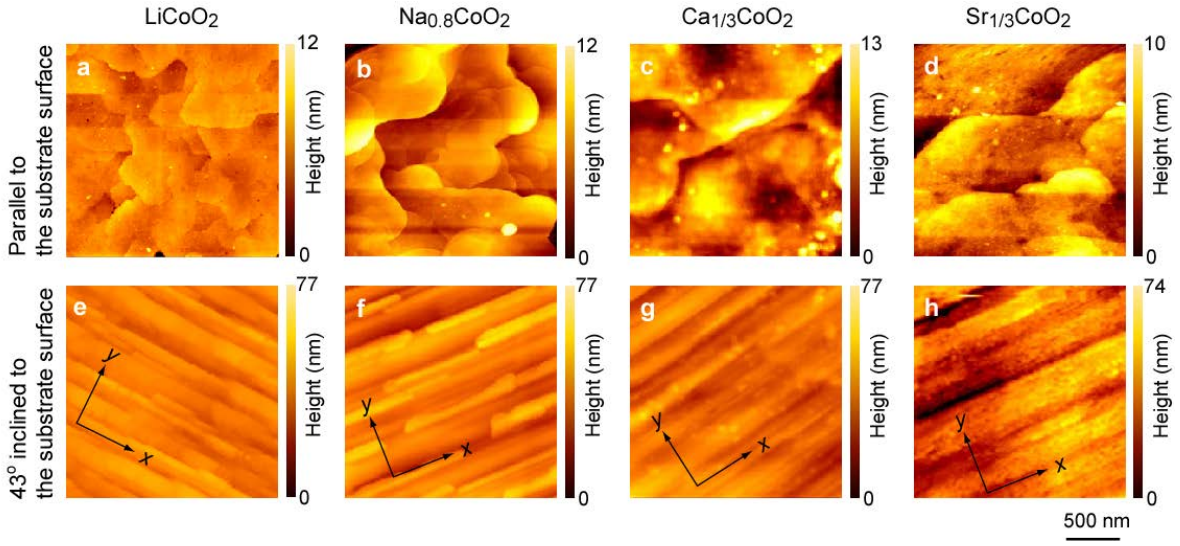

Figure 2. Surface morphology of the films. Topographic AFM images of the A_xCoO_2 films (A = Li, Na, Ca, and Sr). Rather large plate-like grains with atomically flat terraced and stepped surfaces are observed from the films on C-sapphire substrates, while straight stripes corresponding to the cross section of layered structures are seen from the films on M-sapphire substrates.

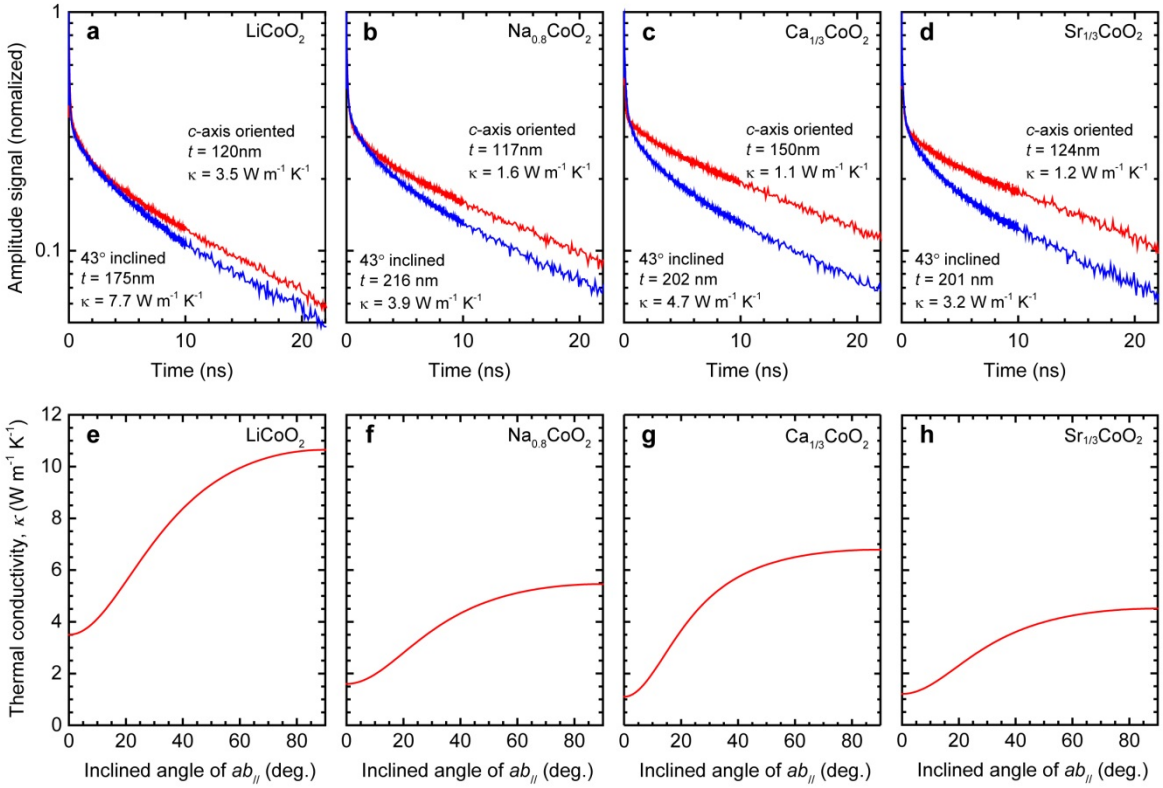

Figure 3. Analyses of the thermal conductivity of the A_xCoO_2 films. Normalized TDTR signals from (a) $LiCoO_2$, (b) $Na_{0.8}CoO_2$, (c) $Ca_{0.33}CoO_2$, and (d) $Sr_{0.33}CoO_2$. The expected measured thermal conductivity from TDTR as a function of the incline angle, calculated from equation (1), are also shown for (e) $LiCoO_2$, (f) $Na_{0.8}CoO_2$, (g) $Ca_{0.33}CoO_2$, and (h) $Sr_{0.33}CoO_2$.

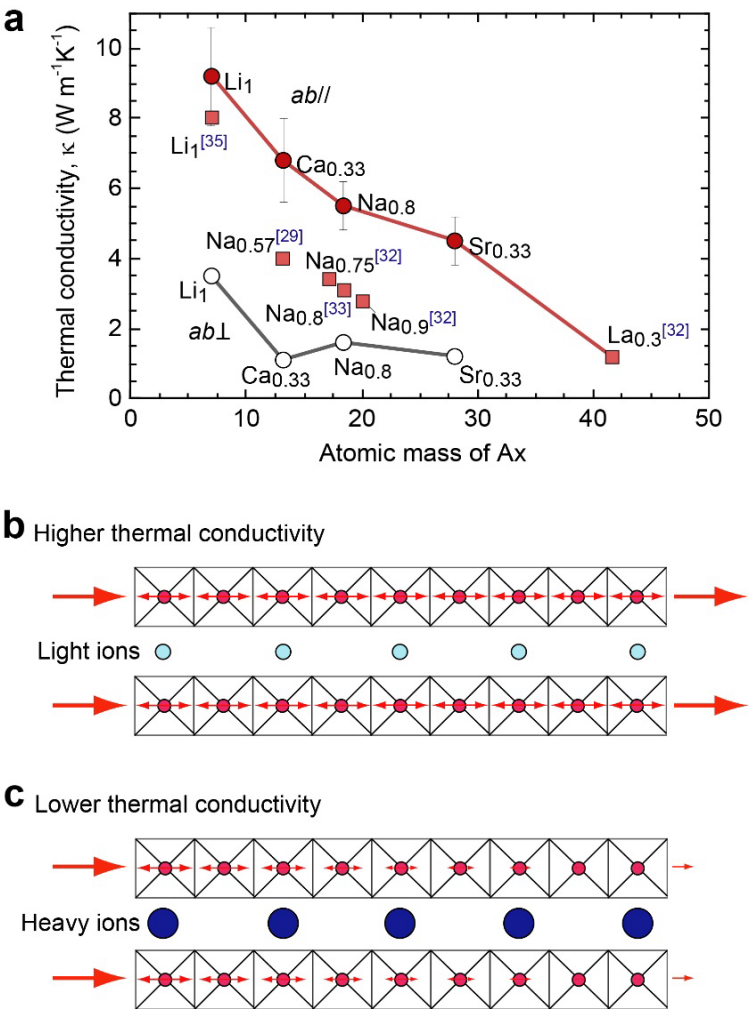

Figure 4. Anisotropic thermal conductivity of the A_xCoO_2. (a) Anisotropic thermal conductivities of A_xCoO_2. The sizes of the error bars of $\kappa_\perp$ were smaller than the circles (**Table I**). $\kappa_{||}$ tends to decrease with the average atomic mass of A_x, but $\kappa_\perp$ only depends on x. These suggests that the main effect of A_x layers on $\kappa_{||}$ comes from the impedance mismatch while $\kappa_\perp$ is dominated by interfacial vacancy scattering of phonons. This difference is likely attributed to the direction of the phonon propagation with respect to the A_x layers. Since $\kappa_\perp$ is related to the heat flux perpendicular to the A_x layers, phonons must transmit through the layers, and the vacancy scatterings and planar densities of A_x will be more important than the impedance mismatch as they are directly related to the phonon scattering cross section.

References

1. Mahan, G.; Sales, B.; Sharp, J., Thermoelectri Materials: New Approaches to an Old Problem. *Phys. Today* **1997,** *50* (3), 42.

2. Snyder, G. J.; Toberer, E. S., Complex thermoelectric materials. *Nature Mater.* **2008,** *7* (2), 105-114.

3. Gelbstein, Y.; Dashevsky, Z.; Dariel, M. P., High performance n-type PbTe-based materials for thermoelectric applications. *Physica B: Condensed Matter* **2005,** *363* (1-4).

4. DiPalma, J., Bismuth toxicity, often mild, can result in severe poisonings. *Emergency Medicine News* **2001,** *23* (3).

5. Jiang, C.; Fan, X.; Feng, B.; Hu, J.; Xiang, Q.; Li, G.; Li, Y.; He, Z., Thermal stability of p-type polycrystalline Bi_2Te_3-based bulks for the application on thermoelectric power generation. *Journal of Alloys and Compounds* **2017,** *692*, 7.

6. Terasaki, I.; Sasago, Y.; Uchinokura, K., Large thermoelectric power in $NaCo_2O_4$ single crystals. *Physical Review B* **1997,** *56*, R12 687.

7. Fujita, K.; Mochida, T.; Nakamura, K., High-Temperature Thermoelectric Properties of $Na_xCoO_{2-\delta}$ Single Crystals. *Jap. J. Appl. Phys.* **2001,** *40*, 4644-4647.

8. Sales, B. C.; Jin, R.; Affholter, K. A.; Khalifah, P.; Veith, G. M.; Mandrus, D., Magnetic, thermodynamic, and transport characterization of $Na_{0.75}CoO_2$ single crystals. *Phys. Rev. B* **2004,** *70* (17), 174419.

9. Ohta, H.; Kim, S. W.; Ohta, S.; Koumoto, K.; Hirano, M.; Hosono, H., Reactive solid-phase epitaxial growth of Na_xCoO_2 (x ~0.83) via lateral diffusion of Na into a cobalt oxide epitaxial layer. *Cryst. Growth Des.* **2005,** *5* (1), 25-28.

10. Lee, M.; Viciu, L.; Li, L.; Wang, Y.; Foo, M. L.; Watauchi, S.; Pascal, R. A., Jr.; Cava, R. J.; Ong, N. P., Large enhancement of the thermopower in Na_xCoO_2 at high Na doping. *Nat. Mater.* **2006,** *5* (7), 537-40.

11. Koshibae, W.; Tsutsui, K.; Maekawa, S., Thermopower in cobalt oxides. *Physical Review B* **2000,** *61*, 6869.

12. Wang, Y.; Rogado, N. S.; Cava, R. J.; Ong, N. P., Spin entropy as the likely source of enhanced thermopower in $Na_xCo_2O_4$. *Nature* **2003,** *423*, 425-428.

13. Takeuchi, T.; Kondo, T.; Takami, T.; Takahashi, H.; Ikuta, H.; Mizutani, U.; Soda, K.; Funahashi, R.; Shikano, M.; Mikami, M.; Tsuda, S.; Yokoya, T.; Shin, S.; Muro, T., Contribution of electronic structure to the large thermoelectric power in layered cobalt oxides. *Phys. Rev. B* **2004,** *69* (12), 125410.

14. Xiang, H. J.; Singh, D. J., Suppression of thermopower of Na_xCoO_2 by an external magnetic field: Boltzmann transport combined with spin-polarized density functional theory. *Phys. Rev. B* **2007,** *76* (19), 195111.

15. Kuroki, K.; Arita, R., "Pudding Mold" Band Drives Large Thermopower in Na_xCoO_2. *J. Phys. Soc. Jap.* **2007,** *76* (8), 083707.

16. Rébola, A.; Klie, R.; Zapol, P.; Öğüt, S., First-principles study of the atomic and electronic structures of misfit-layered calcium cobaltite $(Ca_2CoO_3)(CoO)_{1.62}$ using rational approximants. *Phys. Rev. B* **2012,** *85* (15), 155132.

17. Baran, J. D.; Molinari, M.; Kulwongwit, N.; Azough, F.; Freer, R.; Kepaptsoglou, D.; Ramasse, Q. M.; Parker, S. C., Tuning Thermoelectric Properties of Misfit Layered Cobaltites by Chemically Induced Strain. *J. Phys. Chem. C* **2015,** *119* (38), 21818-21827.

18. Brinks, P.; Kuiper, B.; Breckenfeld, E.; Koster, G.; Martin, L. W.; Rijnders, G.; Huijben, M., Enhanced Thermoelectric Power Factor of NaxCoO2 Thin Films by Structural Engineering. *Adv. Energy Mater.* **2014,** *4* (8), 201301927.

19. Sugiura, K.; Ohta, H.; Nomura, K.; Hirano, M.; Hosono, H.; Koumoto, K., High electrical conductivity of layered cobalt oxide Ca3Co4O9 epitaxial films grown by topotactic ion-exchange method. *Appl. Phys. Lett.* **2006,** *89* (3), 032111.

20. Sugiura, K.; Ohta, H.; Nomura, K.; Hirano, M.; Hosono, H.; Koumoto, K., Fabrication and thermoelectric properties of layered cobaltite, γ-$Sr_{0.32}Na_{0.21}CoO_2$ epitaxial films. *Appl. Phys. Lett.* **2006,** *88*, 082109.

21. Brinks, P.; Heijmerikx, H.; Hendriks, T. A.; Rijnders, G.; Huijben, M., Achieving chemical stability in thermoelectric NaxCoO2 thin films. *Rsc Adv* **2012,** *2* (14), 6023-6027.

22. Cushing, B. L.; Wiley, J. B., Topotactic Routes to Layered Calcium Cobalt Oxides. *J. Solid State Chem.* **(1998),** *141*, 385-391.

23. Guo, Y. Q.; Luo, J. L.; Liu, G. T.; Yang, H. X.; Li, J. Q.; Wang, N. L.; Jin, D.; Xiang, T., Low-temperature magnetic and transport properties of layered Sr_xCoO_2. *Phys. Rev. B* **2006,** *74* (15), 155129.

24. Liu, J.; Huang, X.; Yang, D.; Wan, S.; Xu, G., High-temperature thermoelectric properties of layered Ba_xCoO_2. *Scripta Mater.* **2015,** *100*, 63-65.

25. Ishikawa, R.; Ono, Y.; Miyazaki, Y.; Kajitani, T., Low-temperature synthesis and electric properties of new layered cobaltite, SrxCoO2. *Jpn J Appl Phys 2* **2002,** *41* (3B), L337-L339.

26. Mizutani, A.; Sugiura, K.; Ohta, H.; Koumoto, K., Epitaxial film growth of Li_xCoO_2 ($0.6 \leq x \leq 0.9$) via topotactic ion exchange of $Na_{0.8}CoO_2$. *Cryst. Growth Des.* **2008,** *8*, 755.

27. Sugiura, K.; Ohta, H.; Ishida, Y.; Huang, R.; Saito, T.; Ikuhara, Y.; Nomura, K.; Hosono, H.; Koumoto, K., Structural Transformation of Ca-Arrangements and Carrier Transport Properties in Ca0.33CoO2 Epitaxial Films. *Appl Phys Express* **2009,** *2* (3).

28. Takahata, K.; Terasaki, I., Thermal Conductivity of A_xBO_2-type Layered Oxides $Na_{0.77}MnO_2$ and $LiCoO_2$. *Jap. J. Appl. Phys.* **2002,** *41* (Part 1, No. 2A), 763-764.

29. Rivadulla, F.; Zhou, J. S.; Goodenough, J. B., Chemical, structural, and transport properties of $Na_{1-x}CoO_2$. *Phys. Rev. B* **2003,** *68* (7), 075108.

30. Choi, J.; Manthiram, A., Factors influencing the crystal chemistry of chemically delithiated layered $H_xNi_{1-y-z}Mn_yCo_zO_2$. *J. Mater. Chem.* **2006,** *16* (18), 1726-1733.

31. Sugiura, K.; Ohta, H.; Nakagawa, S.; Huang, R.; Ikuhara, Y.; Nomura, K.; Hosono, H.; Koumoto, K., Anisotropic carrier transport properties in layered cobaltate epitaxial films grown by reactive solid-phase epitaxy. *Appl. Phys. Lett.* **2009,** *94* (15), 152105.

32. Knížek, K.; Hejtmánek, J.; Maryško, M.; Šantavá, E.; Jirák, Z.; Buršík, J.; Kirakci, K.; Beran, P., Structure and properties of a novel cobaltate $La_{0.30}CoO_2$. *J. Solid State Chem.* **2011,** *184* (8), 2231-2237.

33. Voneshen, D. J.; Refson, K.; Borissenko, E.; Krisch, M.; Bosak, A.; Piovano, A.; Cemal, E.; Enderle, M.; Gutmann, M. J.; Hoesch, M.; Roger, M.; Gannon, L.; Boothroyd, A. T.; Uthayakumar, S.; Porter, D. G.; Goff, J. P., Suppression of thermal conductivity by rattling modes in thermoelectric sodium cobaltate. *Nat. Mater.* **2013,** *12* (11), 1028-32.

34. Daou, R.; Frésard, R.; Hébert, S.; Maignan, A., Large anisotropic thermal conductivity of the intrinsically two-dimensional metallic oxide $PdCoO_2$. *Phys. Rev. B* **2015,** *91* (4), 041113(R).

35. Mallick, M. M.; Vitta, S., Giant Enhancement in High-Temperature Thermoelectric Figure-of-Merit of Layered Cobalt Oxide, $LiCoO_2$, Due to a Dual Strategy-Co-Substitution and Lithiation. *Inorg. Chem.* **2017,** *56* (10), 5827-5838.

36. Fujii, S.; Yoshiya, M.; Yumura, A.; Miyauchi, Y.; Tada, M.; Yasuda, H., Impact of dynamic interlayer interactions on thermal conductivity of $Ca_3Co_4O_9$. *J. Electron. Mater.* **2014,** *43*, 1905-1915.

37. Fujii, S.; Yoshiya, M.; Fisher, C. A. J., Quantifying anharmonic vibrations in thermoelectric layered cobaltites and their role in suppressing thermal conductivity. *Sci. Rep.* **2018,** *8*, 11152.

38. Tang, X.; Aaron, K.; He, J.; Tritt, T. M., Determination of in-plane thermal conductivity of $Na_xCo_2O_4$ single crystals via a parallel thermal conductance (PTC) technique. *phys. stat. sol. (a)* **2008,** *205* (5), 1152-1156.

39. Ohta, H.; Mizutani, A.; Sugiura, K.; Hirano, M.; Hosono, H.; Koumoto, K., Surface modification of glass substrates for oxide heteroepitaxy: Pasteable three-dimensionally oriented layered oxide thin films. *Adv. Mater.* **2006,** *18* (13), 1649.

40. Motohashi, T.; Ono, T.; Katsumata, Y.; Kanno, R.; Karppinen, M.; Yamauchi, H., Electrochemical synthesis and properties of CoO_2, the x = 0 phase of the A_xCoO_2 systems (A = Li, Na). *Journal of Applied Physics* **2008,** *103*.

41. Cho, H. J.; Kim, G.; Onozato, T.; Jeen, H.; Ohta, H., Thermal conductivity tensor of NbO_2. *Int. J. Heat Mass Transf.* **2019,** *137*, 263-267.

42. He, H.; Zhang, L.; Liu, L., Thermal transport in monocrystalline and polycrystalline lithium cobalt oxide. *Physical Chemistry Chemical Physics* **2019,** *21*, 121192.

43. Yang, H.; Yang, J.-y.; Savory, C. N.; Skelton, J. M.; Morgan, B. J.; Scanlon, D. O.; Walsh, W., Highly anisotropic thermal transport in $LiCoO_2$. *Journal of Physical Chemistry Letters* **2019,** *10* (18), 5.

44. Baran, J. D.; Kepaptsoglou, D.; Molinari, M.; Kulwongwit, N.; Azough, F.; Freer, R.; Ramasse, Q. M.; Parker, S. C., Role of structure and defect chemistry in high-performance thermoelectric bismuth strontium cobalt oxides. *Chemistry of Materials* **2016,** *28*, 9.

45. Azough, F.; Jackson, S. S.; Ekren, D.; Freer, R.; Molinari, M.; Yeandel, S. R.; Panchmatia, P. M.; Parker, S. C.; Maldonado, D. H.; Kepaptsoglou, D. M.; Ramasse, Q. M., Concurrent La and A-site vacancy doping modulates the thermoelectric response of $SrTiO_3$: experimental and computational evidence. *ACS Applied Materials & Interfaces* **2017,** *9*, 13.

46. Baran, J. D.; Molinari, M.; Kulwongwit, N.; Azough, F.; Freer, R.; Kepaptsoglou, D.; Ramasse, Q. M.; Parker, S. C., Tuning Thermoelectric Properties of Misfit Layered Cobaltites by Chemically Induced Strain. *The Journal of Physical Chemistry C* **2015,** *119* (38), 21818-21827.

47. Kittel, C., *Introduction to solid state physics*. Wiley: Hoboken, NJ, 2005.

Anisotropic heat conduction of ion substituted layered cobalt oxides has been clarified by measuring the thermal conductivity of the epitaxial films with two different crystallographic orientations against the surface normal to the substrates. The result “heavy ion substitution suppresses the anisotropy of heat conduction” would provide new materials design concept for good thermoelectrics.

Keyword anisotropy, thermal conductivity, thermoelectric properties, layered cobalt oxides, epitaxial films

H.J. Cho*, Y. Takashima, Y. Nezu, T. Onozato, H. Ohta*

Anisotropic Heat Conduction in Ion Substituted Layered Cobalt Oxides

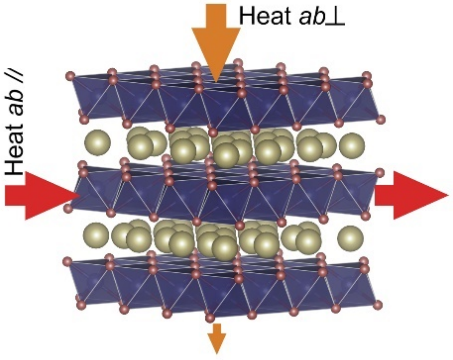

Copyright WILEY-VCH Verlag GmbH & Co. KGaA, 69469 Weinheim, Germany, 2016.

Supporting Information

Anisotropic Heat Conduction in Ion Substituted Layered Cobalt Oxides

Hai Jun Cho, Yugo Takashima, Yukio Nezu, Takaki Onozato, and Hiromichi Ohta**

Prof. H.J. Cho, Prof. H. Ohta
Research Institute for Electronic Science, Hokkaido University, N20W10, Kita, Sapporo 001−0020, Japan
E-mail: joon@es.hokudai.ac.jp, hiromichi.ohta@es.hokudai.ac.jp
Prof. H.J. Cho, Y. Takashima, Y. Nezu, T. Onozato, Prof. H. Ohta
Graduate School of Information Science and Technology, Hokkaido University, N14W9, Kita, Sapporo 060−0814, Japan

Keywords: anisotropy, thermal conductivity, thermoelectric properties, layered cobalt oxides, epitaxial films

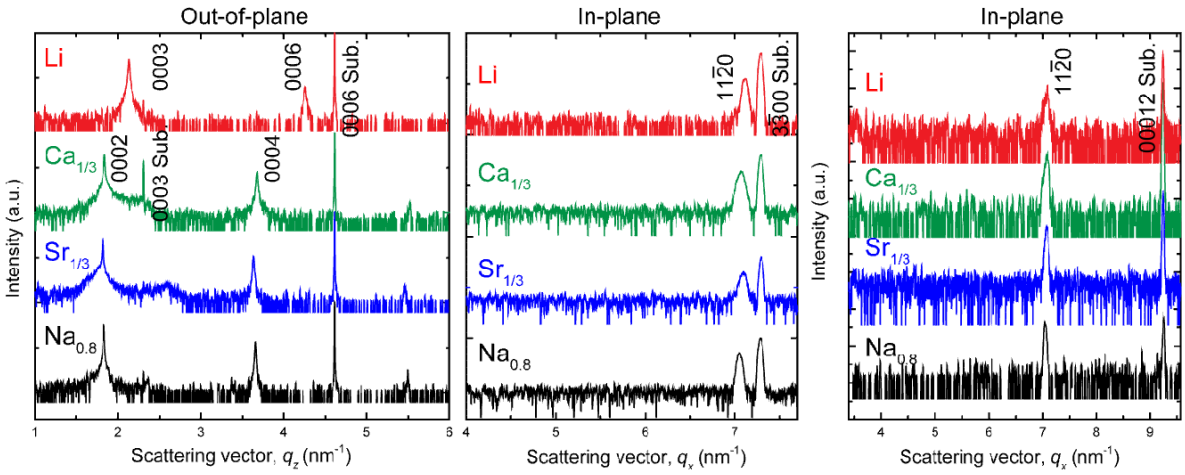

Figure S1. Epitaxial relationships between A_xCoO_2 films and the substrates. XRD patterns of the A_xCoO_2 films (A = Li, Na, Ca, and Sr) fabricated on C- and M-sapphire substrates. Strong out-of-plane diffraction peaks are observed, and the peak locations suggest the formation of $LiCoO_2$, $Ca_{0.33}CoO_2$, $Sr_{0.33}CoO_2$, and $Na_{0.8}CoO_2$, which are consistent with previous studies. [9,25,27,40]

Through-plane thermal conductivity of layered structures oberved in TDTR

In a tilted layered film with a thickness *t*, define a Cartesian coordinate system ($\hat{x}$, $\hat{y}$, $\hat{z}$) such that the tilt angle θ be in the *xz* plane (**Figure S2**). Consider a steady state heat flux along $\hat{z}$ from the top of the film. Let T_1 and T_2 denote the steady state temperatures of the top and the bottom of the film, respectively. For simplicity, assume that the temperature gradient is linear Along $\hat{z}$. In other words, $\vec{\nabla}T = (0,0,\nabla T_z)$.

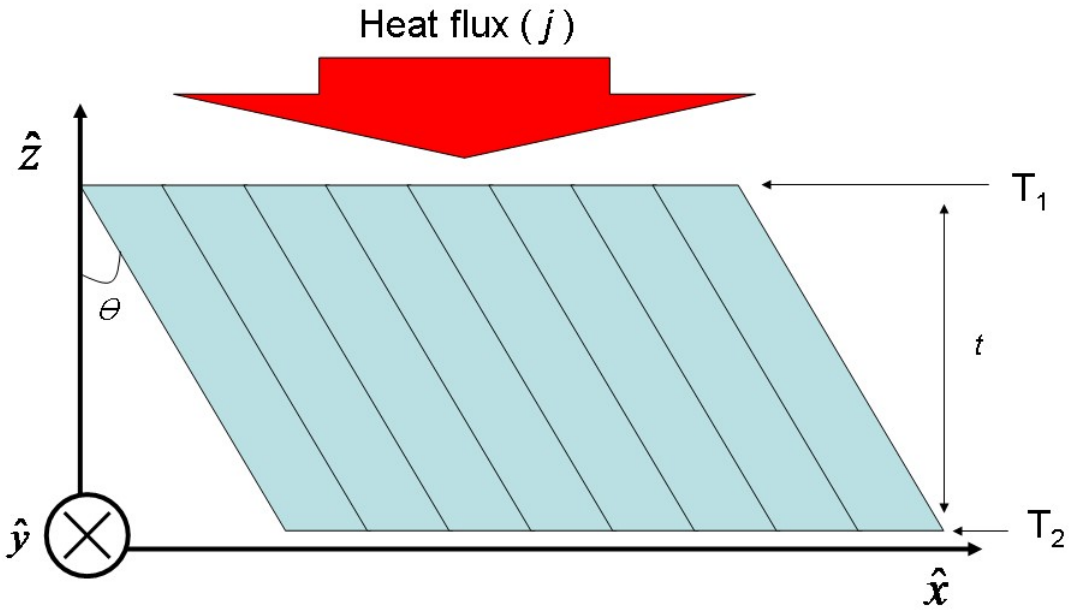

Figure S2: Schematic diagram showing a steady state heat flux in a layered structure at an angle θ. *t* denotes the thickness of the film. For simplicity, the temperature gradient was assumed to be linear along *z*.

The steady state heat flux can be expressed as:

$$\vec{j} = \begin{pmatrix} j_x \\ j_y \\ j_z \end{pmatrix} = -\kappa\vec{\nabla}T = -\begin{pmatrix} \kappa_{xx} & \kappa_{xy} & \kappa_{xz} \\ \kappa_{yx} & \kappa_{yy} & \kappa_{yz} \\ \kappa_{zx} & \kappa_{zy} & \kappa_{zz} \end{pmatrix}\begin{pmatrix} 0 \\ 0 \\ \nabla T_z \end{pmatrix} = -\begin{pmatrix} \kappa_{xz}\nabla T_z \\ \kappa_{yz}\nabla T_z \\ \kappa_{zz}\nabla T_z \end{pmatrix} \quad (1)$$

The TDTR laser spot radius (34 μm) is much greater than the thermal diffusive wavelength in all directions (< 1 μm). Therefore, in-plane heat diffusion will be small compare to the heat propagating away from the front surface. Since the layered structure is tiled in the *xz* plane, the heat flux along *y* will be negligible.

Therefore, $j_y = \kappa_{zy} = 0$, and

$$\vec{j} = \begin{pmatrix} j_x \\ 0 \\ j_z \end{pmatrix} = -\begin{pmatrix} \kappa_{xz}\nabla T_z \\ 0 \\ \kappa_{zz}\nabla T_z \end{pmatrix} \qquad (2)$$

Substituting $\nabla T_z = \frac{T_1 - T_2}{t}$ yields:

$$j_x = \kappa_{xz}\frac{T_1 - T_2}{t},\ j_z = \kappa_{zz}\frac{T_1 - T_2}{t} \qquad (3)$$

Since j_x and j_z can be decomposed into the heat fluxes parallel and perpendicular to the layers (**Figure S3**).

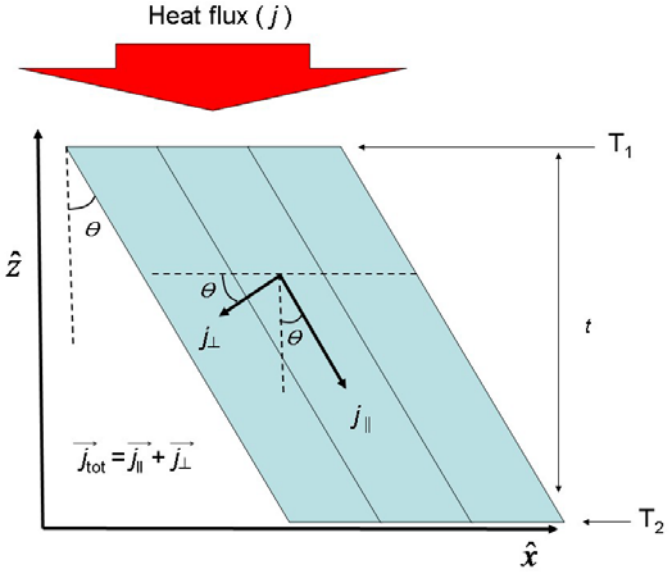

Figure S3: Schematic diagram showing a steady state heat flux decomposed into components parallel and perpendicular to the layers.

The heat flux parallel to the layers ($j_\parallel$) is given by:

$$j_\parallel = \kappa_\parallel|\nabla T_\parallel| = \kappa_\parallel\frac{T_1 - T_2}{t/cos\theta} \qquad (4)$$

where $\kappa_\parallel$ and $\nabla T_\parallel$ are the thermal conductivity and the temperature gradient parallel to the layers, respectively. Similarly, the heat flux perpendicular to the layers ($j_\perp$) is given by:

$$j_\perp = \kappa_\perp|\nabla T_\perp| = \kappa_\perp\frac{T_1 - T_2}{t/sin\theta} \qquad (5)$$

where $\kappa_\perp$ and $\nabla T_\perp$ are the thermal conductivity and the temperature gradient perpendicular to the layers, respectively.

From Fig. S3,

$$j_z = j_{\parallel} cos\theta + j_{\perp} sin\theta \qquad (6)$$

Substituting equations (4) and (5) into equation (6) gives

$$j_z = \kappa_{\parallel} \left(\frac{T_1 - T_2}{t}\right) cos^2\theta + \kappa_{\perp} \left(\frac{T_1 - T_2}{t}\right) sin^2\theta = (\kappa_{\parallel} cos^2\theta + \kappa_{\perp} sin^2\theta) \left(\frac{T_1 - T_2}{t}\right) \qquad (7)$$

κ_{zz} can be obtained from comparing equations (3) and (7).

$$\kappa_{zz} = \kappa_{\parallel} cos^2\theta + \kappa_{\perp} sin^2\theta \qquad (8)$$

Note $\kappa_{zz} = \kappa_{\parallel}$ if θ = 0 °, and $\kappa_{zz} = \kappa_{\perp}$ if θ = 90 °.

Similarly, for j_x,

$$j_x = j_{\parallel} sin\theta - j_{\perp} cos\theta \qquad (9)$$

Substituting equations (4) and (5) into equation (9) gives

$$j_x = \kappa_{\parallel} \left(\frac{T_1 - T_2}{t}\right) cos\theta sin\theta + \kappa_{\perp} \left(\frac{T_1 - T_2}{t}\right) cos\theta sin\theta = (\kappa_{\parallel} - \kappa_{\perp}) \left(\frac{T_1 - T_2}{t}\right) cos\theta sin\theta \qquad (10)$$

κ_{zz} can be obtained from comparing equations (3) and (10).

$$\kappa_{xz} = (\kappa_{\parallel} - \kappa_{\perp}) cos\theta sin\theta \qquad (11)$$

Note κ_{xz} = 0 if $\kappa_{\parallel} = \kappa_{\perp}$ (isotropy), which is expected from an isotropic material. In addition, κ_{xz} = 0 if θ = 0 ° or 90 °.

The obsreved thermal conductivity (κ_{obsd}) from the TDTR is attributed to the total heat flux.

Therefore, the total heat flux (j_{tot}) needs to be obtained from equations (7) and (10).

$$j_{tot} = \sqrt{{j_x}^2 + {j_z}^2} = \left(\frac{T_1 - T_2}{t}\right) \sqrt{(\kappa_{\parallel} cos^2\theta + \kappa_{\perp} sin^2\theta)^2 + (\kappa_{\parallel} - \kappa_{\perp})^2 cos^2\theta sin^2\theta} \qquad (12)$$

The relationship between the total heat flux and the measured thermal conductivity can be expressed by:

$$j_{tot} = \kappa_{obsd}|\nabla T| \qquad (13)$$

Combining equations (12) and (13) yields

$$\kappa_{obsd} = \frac{j_{tot}}{|\nabla \mathrm{T}|} = \sqrt{(\kappa_{\parallel} cos^2\theta + \kappa_{\perp} sin^2\theta)^2 + (\kappa_{\parallel} - \kappa_{\perp})^2 cos^2\theta sin^2\theta}$$

$$= \sqrt{{\kappa_{\parallel}}^2 cos^2\theta + {\kappa_{\perp}}^2 sin^2\theta} \qquad (14)$$

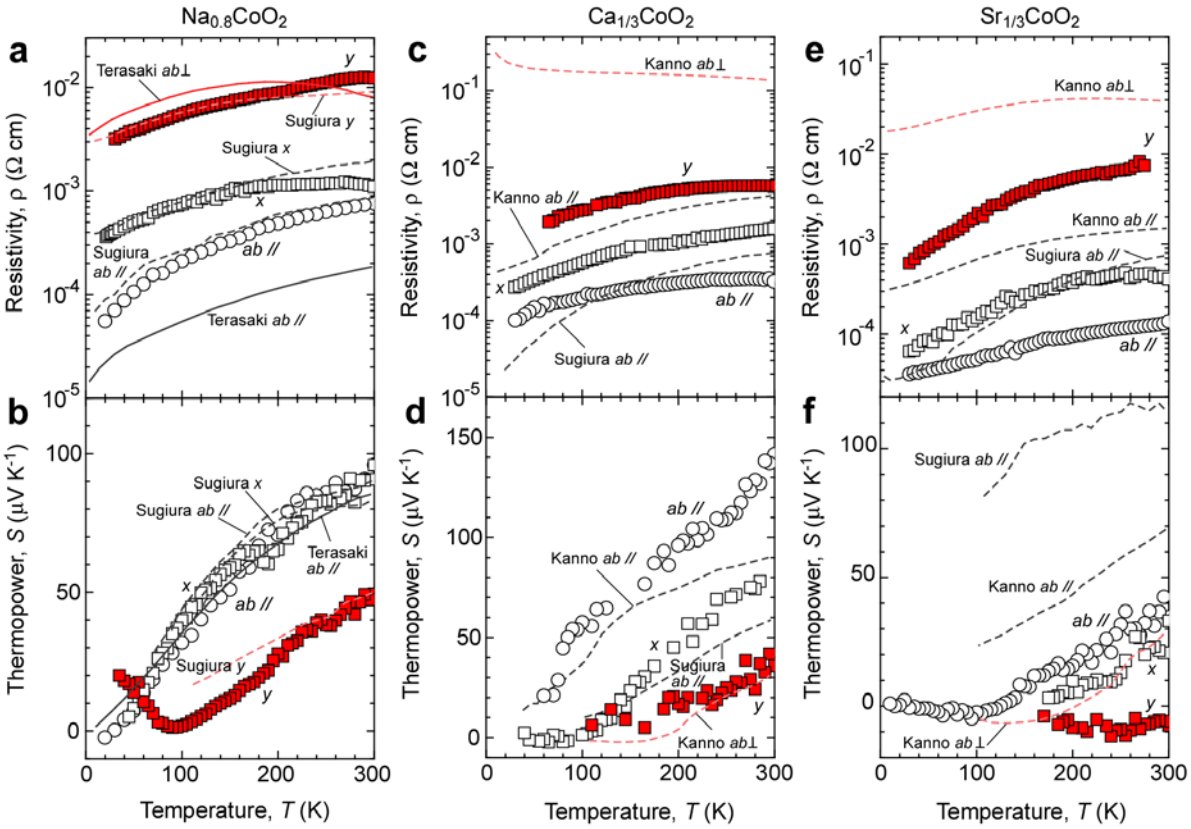

Figure S4. Thermoelectric properties (upper: resistivity, lower: thermopower) of (a, b) $Na_{0.8}CoO_2$, (c, d) $Ca_{0.33}CoO_2$, and (e, f) $Sr_{0.33}CoO_2$ films. All electrical properties were measured in vacuum to prevent the effect of moisture. $LiCoO_2$ did not conduct electricity.